AIP | Journal of Applied Physics

Bandgap engineering of Cu2CdxZn1−xSnS4 alloy for photovoltaic applications: A complementary experimental and first-principles study

Zhen-Yu Xiao, Yong-Feng Li, Bin Yao, Rui Deng, Zhan-Hui Ding, Tom Wu, Gang Yang, Chun-Ran Li, Zi-Yuan Dong, Lei Liu, Li-Gong Zhang, and Hai-Feng Zhao

Citation: Journal of Applied Physics **114**, 183506 (2013); doi: 10.1063/1.4829457
View online: http://dx.doi.org/10.1063/1.4829457
View Table of Contents: http://scitation.aip.org/content/aip/journal/jap/114/18?ver=pdfcov
Published by the AIP Publishing

Bandgap engineering of $Cu_2Cd_xZn_{1-x}SnS_4$ alloy for photovoltaic applications: A complementary experimental and first-principles study

Zhen-Yu Xiao,[1] Yong-Feng Li,[1,a)] Bin Yao,[2,a)] Rui Deng,[3] Zhan-Hui Ding,[2] Tom Wu,[4] Gang Yang,[1] Chun-Ran Li,[1] Zi-Yuan Dong,[1] Lei Liu,[5] Li-Gong Zhang,[5] and Hai-Feng Zhao[5]
[1]*Key Laboratory of Physics and Technology for Advanced Batteries (Ministry of Education), College of Physics, Jilin University, Changchun 130012, China*
[2]*State Key Laboratory of Superhard Material and College of Physics, Jilin University, Changchun 130012, China*
[3]*School of Materials Science and Engineering, Changchun University of Science and Technology, Changchun 130022, China*
[4]*Physical Sciences and Engineering Division, Solar and Photovoltaics Engineering Research Center, King Abdullah University of Science and Technology, Thuwal 23955-6900, Saudi Arabia*
[5]*State Key Laboratory of Luminescence and Applications, Changchun Institute of Optics, Fine Mechanics and Physics, Chinese Academy of Sciences, No.3888 Dongnanhu Road, Changchun 130033, China*

(Received 18 August 2013; accepted 22 October 2013; published online 11 November 2013)

We report on bandgap engineering of an emerging photovoltaic material of $Cu_2Cd_xZn_{1-x}SnS_4$ (CCZTS) alloy. CCZTS alloy thin films with different Cd contents and single kesterite phase were fabricated using the sol-gel method. The optical absorption measurements indicate that the bandgap of the kesterite CCZTS alloy can be continuously tuned in a range of 1.55–1.09 eV as Cd content varied from $x = 0$ to 1. Hall effect measurements suggest that the hole concentration of CCZTS films decreases with increasing Cd content. The CCZTS-based solar cell with $x = 0.47$ demonstrates a power conversion efficiency of 1.2%. Our first-principles calculations based on the hybrid functional method demonstrate that the bandgap of the kesterite CCZTS alloy decreases monotonically with increasing Cd content, supporting the experimental results. Furthermore, Cu_2ZnSnS_4/Cu_2CdSnS_4 interface has a type-I band-alignment with a small valence-band offset, explaining the narrowing of the bandgap of CCZTS as the Cd content increases. Our results suggest that CCZTS alloy is a potentially suitable material to fabricate high-efficiency multi-junction tandem solar cells with different bandgap-tailored absorption layers. © *2013 AIP Publishing LLC*. [http://dx.doi.org/10.1063/1.4829457]

I. INTRODUCTION

At present, facing the increasingly serious global energy crisis, it is of pressing importance for material research to explore environment-friendly, low cost, and high-efficiency solar cells.[1–3] Among various kinds of solar cells, the $CuIn_{1-x}Ga_xSe_2$ (CIGS) thin-film solar cell has been paid much attentions due to its high power conversion efficiency and stability.[4,5] However, the high costs of gallium and indium obstruct the further development in the field of thin-film solar cell.[6] In recent years, some efforts have been made to find low cost materials with earth-abundant elements. Cu_2ZnSnS_4 (CZTS), as a potential material to substitute CIGS, has attracted great interest due to its direct bandgap ($E_g \sim 1.5$ eV) with high absorption coefficient and earth-abundant elements.[7–16] Very recently, it has been reported that a CZTS thin-film solar cell with a conversion efficiency of 9.2%, which is a new efficiency record for such solar cells.[17]

To further improve the efficiency of CZTS-based solar cells, a good choice is to fabricate multi-junction solar cells because different bandgaps of various junctions can hopefully span the whole wavelength range in the solar spectrum. For example, alloys of $CuIn_{1-x}Ga_xSe_2$, $In_xGa_{1-x}P$, and $In_xGa_{1-x}As$ have been used to fabricate multi-junction solar cells due to the tunable bandgap by controlling the In content.[18–21] Therefore, it is important to find a bandgap-tunable material based on CZTS for realizing the future low-cost tandem solar cells with earth-abundant elements. Furthermore, the band offset at interface is one of the most fundamentally physical parameters, which is often used to assess some important interface effects, i.e., quantum confinement and carrier transport, in particular, for the design of solar cells and other optoelectronic devices. Therefore, it is necessary to obtain a clear understanding of valence-band (VB) electronic structures and valence-band maximum (VBM) shift of CZTS-based alloys.

In this work, we synthesized $Cu_2Cd_xZn_{1-x}SnS_4$ (CCZTS, $0 \le x \le 1$) alloy thin films to realize the goal of bandgap engineering in CZTS-based solar cells. Experimentally, the bandgap of the CCZTS alloy can be tuned in a range of 1.55–1.09 eV by changing the Cd content, suggesting that CCZTS alloy is a potentially suitable material to fabricate high-efficient multi-junction solar cells with different bandgap-tailored absorption layers. In addition, since the CCZTS alloy shows *p*-type conduction with hole carriers, the VBM position affects the acceptor level and the hole carrier transport. Complementarily, we carried out first-principles calculations based on the hybrid functional method to obtain

a)Electronic addresses: liyongfeng@jlu.edu.cn and binyao@jlu.edu.cn

the valence-band offset of CZTS/Cu_2CdSnS_4 (CCTS), which is well explained by the *p-d* repulsion effect.

II. EXPERIMENTAL METHODS AND FIRST-PRINCIPLES CALCULATIONS DETAIL

A. Experimental methods

The CCZTS alloy thin films were synthesized on the soda lime glass (SLG) substrates using the sol-gel methods. First, the solutions of the CCZTS precursors were prepared from copper (II) acetate monohydrate, zinc (II) acetate dihydrate, tin (II) chloride dihydrate, cadmium (II) chloride, thiourea, 2-methoxyethanol (2-metho), and monoethanolamine (MEA). The 2-metho and MEA were used as the solvent and the stabilizer, respectively. The mole ratios of Cu, (Cd + Zn), Sn, and S in the solution are 2:1:1:4. For obtaining the solution with the different Cd contents, the mole ratios of Cd to (Cd + Zn) in the solution are varied as 0, 0.1, 0.3, 0.5, 0.8, and 1. The solution was stirred at 45 °C to completely dissolve the metal compounds. Then, the solution was dropped onto the SLG substrate that was rotating at 3000 rpm for 30 s. After deposition by spin coating, the films ware dried in air at 300 °C. The coating and drying processes were repeated for five times to obtain 2-μm-thick films. Figure 1 shows a typical cross-section SEM image of the CCZTS alloy thin film. To study the performance of solar cells based on CCZTS films, we prepared two prototype devices of CCZTS solar cells with the Cd content of 0 and 0.47, respectively, denoted as devices A and B, respectively. The CCZTS layers were first synthesized on SLG substrates with precoated Mo layers using the sol-gel method. The CdS, ZnO, and ZnO:Al layers were successively deposited on CCZTS layers using magnetron sputtering to obtain prototype devices with a structure of ZnO:Al/ZnO/CdS/CCZTS/Mo. The Al content in ZnO:Al target is 3%. The detailed growth conditions of CdS, ZnO and ZnO:Al films can be found elsewhere.[22,23]

The crystal structures of the CCZTS alloy films were characterized by an X-ray diffractometer (XRD) with Cu K_α radiation ($\lambda = 1.5406$ Å). The room temperature optical absorption measurements were performed using an UV-visible-near infrared spectrophotometer. The x-ray photoelectron spectroscopy (XPS) measurements were carried out using an ESCALAB 250 XPS instrument with Al $K_\alpha = 1486.6$ eV x-ray radiation source and all XPS spectra were calibrated by the C1s peak (284.6 eV). Electrical properties and carrier concentrations were characterized with the van der Pauw configuration in a Hall effect measurement system. For the power conversion efficiency measurements of CCZTS-based solar cells, the current density-voltage curves were measured under simulated AM1.5 solar illumination with an intensity of 100 mW/cm^2 using an AAA class solar simulator.

B. First-principles calculations detail

To better understand the narrow of the bandgap with increasing Cd content, we calculated electronic structure of CCZTS alloy and valence-band offset of CZTS/CCTS based on the first-principles method. The first-principles calculations were performed using the plane-wave projector augmented-wave (PAW) method[24,25] applying the semilocal Perdew-Burke-Ernzerhof (PBE) exchange-correlation functional[26] and the Heyd-Scuseria-Ernzerhof (HSE) hybrid functional[27] as implemented in the VASP code.[28,29] We constructed a 64-atom CZTS supercell with the kesterite structure. To study the possible Cd substitution, we first checked the formation energies of Cd substituting for Cu (Cd_{Cu}), Zn (Cd_{Zn}) and Sn (Cd_{Sn}) in CZTS, respectively. It was found the Cd_{Zn} has the lowest formation energy, in agreement with the calculation by Maeda *et al.*[30] To simulate the CCZTS alloy, different numbers of Zn atoms in the CZTS lattice were substituted by Cd atoms, corresponding to x = 0, 0.125, 0.25, 0.5, 0.75, and 1, respectively.

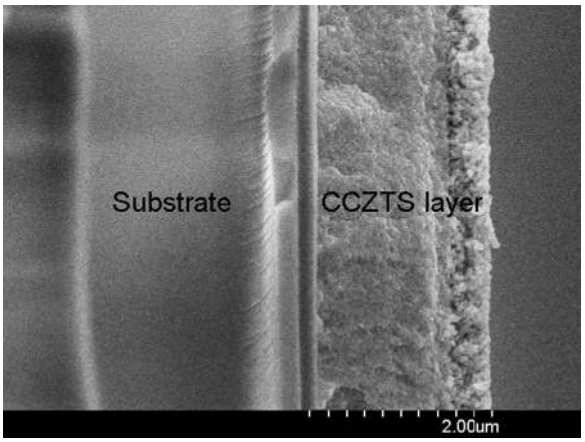

FIG. 1. A typical cross-section SEM image of the $Cu_2Cd_xZn_{1-x}SnS_4$ alloy thin film with a thickness of ~2 μm.

For the calculation of valence-band offset (VBO) in Cu_2ZnSnS_4/Cu_2CdSnS_4 (CZTS/CCTS), we adopted the following formula:[31–35]

$$\Delta E_V = \Delta E_{CL} + (E_{CL}^{CZTS} - E_{VBM}^{CZTS}) - (E_{CL}^{CCTS} - E_{VBM}^{CCTS}), \quad (1)$$

where ΔE_{CL} is the difference of core levels between CZTS and CCTS in the CZTS/CCTS superlattice, the second and third terms are the energy difference between core level and VBM for the bulk CZTS and CCTS, respectively. Here, we adopted the average electrostatic potential as the core level to align the valence-band because the average electrostatic potential in the core region can be used to determine the core level shift. We constructed three structures, bulk CZTS, CCTS, and CZTS/CCTS superlattice for calculating the VBO of CZTS/CCTS. The bulk CZTS and CCZT were first calculated separately to determine the valence-band maximum (E_{VBM}) with respect to the corresponding E_{AEP} in the bulk, and then, a $1 \times 1 \times 4$ CZTS/CCTS [001] superlattice was constructed and the E_{AEP} on both sides were extracted. In the calculation, the cutoff energy for the plane-wave basis set is 500 eV. The atoms are allowed to relax until the Hellmann–Feynman forces acting on them become smaller than 0.01 eV/Å.

III. RESULTS AND DISCUSSION

A. Composition, structure, and Cd chemical state of CCZTS films

The element ratios of the CCZTS alloy films were determined by XPS measurements and are listed in Table I. It is

TABLE I. Composition ratios of the $Cu_2Cd_xZn_{1-x}SnS_4$ alloy thin films.

	Composition ratios in films			
Cd/(Cd + Zn) in solution	Cd/(Cd + Zn)	Cu/(Zn + Cd + Sn)	(Cd + Zn)/Sn	S/metal
0	0	0.92	1.00	0.70
0.1	0.14	0.75	0.84	0.68
0.3	0.35	0.86	0.95	0.69
0.5	0.47	0.62	1.18	0.70
0.8	0.50	0.73	1.66	0.56

found that the Cd/(Cd + Zn) ratio in the films increases on increasing Cd content in the solutions. All films show the Cu-poor compositions. It was reported that Cu-poor conditions can improve the efficiency of the CZTS-based solar cells because of the formation of Cu vacancies, which gives rise to shallow acceptors.[36]

Figure 2(a) shows the XRD patterns of the CCZTS alloy thin films. For all films, there are three diffraction peaks, which are attributed to the diffraction of the (112), (220), and (312) planes of the kesterite structure. The enlarged (112) diffraction peaks are shown in Fig. 2(b). With the increase of Cd content, the diffraction peak monotonously shifts towards small angles, indicating that the lattice constant increases. The expansion of lattice constant is attributed to the larger Cd ion radius than Zn. The *a*- and *c*-axis lattice constants were calculated from the XRD data, as shown in Fig. 2(c). The *a*-axis lattice constant increases from 0.539 to 0.553 nm as the Cd content increases from 0 to 1. Concurrently, the *c*-axis lattice constant also increases from 1.078 to 1.113 nm. Empirically, the relation between the lattice constants and the Cd content follows linear behavior: $a(x) = 0.539 + 0.015x$ and $c(x) = 1.076 + 0.033x$. As an initial test, the geometry-optimized a- and c-axis lattice constants based on first-principles calculation are 0.547 and 1.093 nm for CZTS, respectively, which are slightly higher than our experimental values by ~1.4% and consistent with the calculated result by Paier *et al.*[37] To compare with the experimental results, the calculated lattice constants of the CCZTS are also shown in Fig. 2(c). As increasing Cd content, the calculated a- and c-axis lattice constants increase, in agreement with the XRD results, indicating that Cd mostly substitutes for Zn.

Fig. 3(a) shows the Raman spectra of the CCZTS alloys thin films. All the spectra exhibit the peaks of the A_1 mode expected for the kesterite structure.[13] The enlarged A_1 mode peaks are shown in Fig. 3(b), which clearly demonstrate that the peaks of the A_1 mode systematically shift to lower wave number with the increase of Cd content. The progressive Raman shift of the A_1 modes as a function of Cd content is shown in Fig. 3(c). This systematic shift in the Raman peaks can be attributed to the lattice expansion as Cd is alloyed into CZTS.

To determine the chemical state of Cd in CCZTS, we performed the XPS measurements. Figure 4 shows the Cd 3*d* high-resolution XPS spectrum of the CCZTS film with the Cd content of 0.47. The Cd $3d_{3/2}$ and Cd $3d_{5/2}$ peaks locate at 405.22 and 411.98 eV, respectively, and the peak splitting of 6.8 eV suggests that the chemical valence of Cd is +2.[38–40] The simplest substitution is that the Cd substitutes metal sites in CCZTS, including Cd_{Zn}, Cd_{Cu}, and Cd_{Sn}, respectively. According to the chemical valence of Cd, Cd_{Zn} is an isoelectronic substitution and Cd_{Cu} is donor-type, whereas Cd_{Sn} is acceptor-type. However, as discussed in Sec. II B, our calculations of the formation energies of the substitution doping suggest that the Cd_{Zn} has the lowest formation energy in the three substitutions. Therefore, most likely consequence of the Cd doping is the isoelectronic substitution of the Zn sites.

B. Optical bandgap of CCZTS films

To obtain the dependence of the bandgap on the Cd content, we performed the optical absorption measurements for

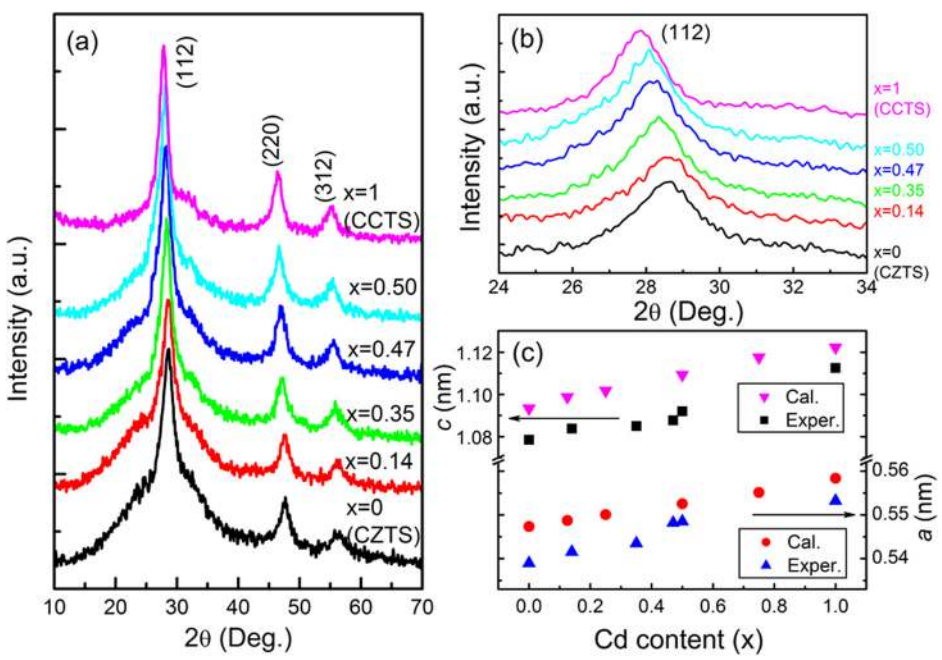

FIG. 2. (a) XRD patterns and (b) enlarged view of the corresponding (112) diffraction peaks of the $Cu_2Cd_xZn_{1-x}SnS_4$ alloy thin films with different Cd contents. (c) Lattice constant as a function of the Cd content as derived from the first-principles calculations and the XRD data.

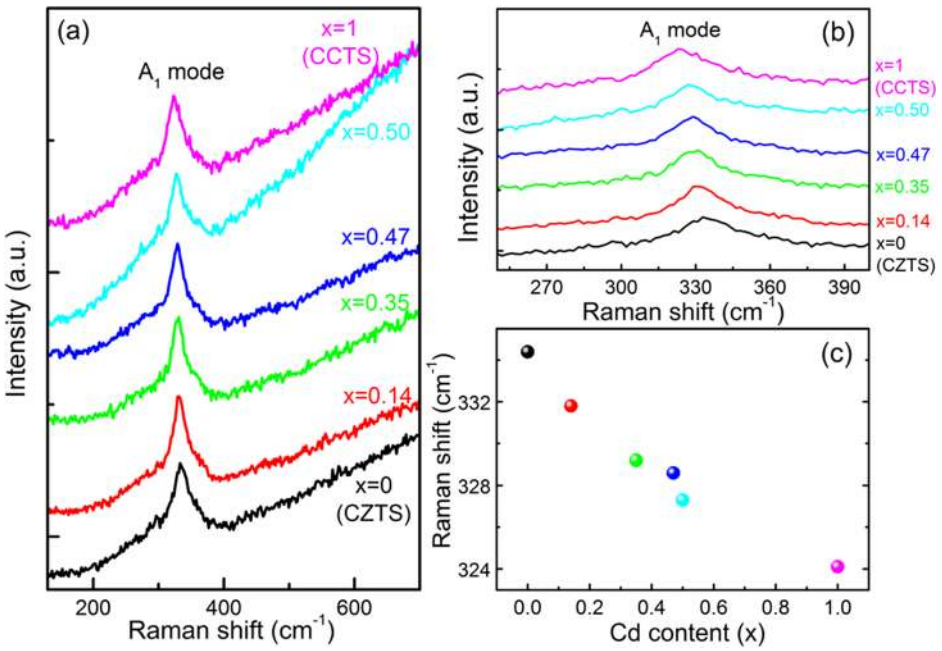

FIG. 3. (a) Raman spectra of the $Cu_2Cd_xZn_{1-x}SnS_4$ alloy films. (b) Corresponding enlarged region of the A_1 mode. (c) Raman shift of the A_1 mode as a function of the Cd content.

the CCZTS alloy films. Figure 5(a) shows the square of the optical absorption coefficient (α^2) versus photon energy (hv) for all the samples. Using the relation: $\alpha(hv) \propto (hv\text{-}E_g)^{1/2}$,[41,42] the optical bandgaps (E_g) are estimated to be 1.55, 1.45, 1.36, 1.27, 1.22, and 1.09 eV for the CCZTS alloy thin films with the Cd contents of 0, 0.14, 0.35, 0.47, 0.5, and 1, respectively. The obtained optical bandgaps for the CZTS and CCTS are consistent with the previous reports.[11,43,44] The yielded optical bandgaps as a function of Cd content are shown in Fig. 5(b). The linear dependence can be written as

$$E_g(x) = 1.531 - 0.462x. \quad (2)$$

Based on this result, we can predict that CCZTS films with tunable bandgaps may be used in future multi-junction solar cells covering a wavelength range of 810–1160 nm. Such tandem solar cells with different bandgap-tailored absorption layers are promising to improve the conversion efficient.

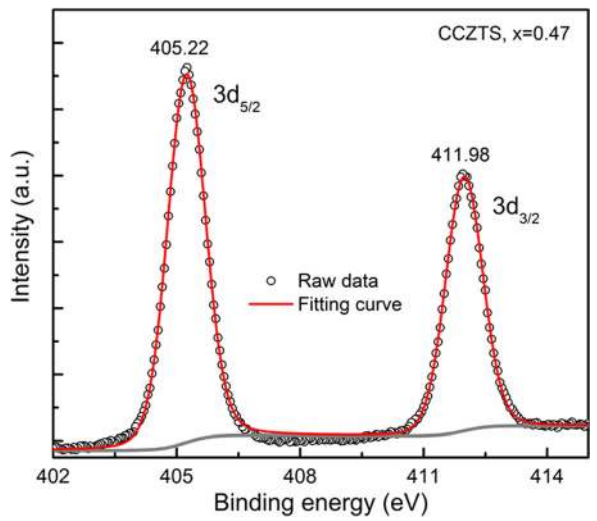

FIG. 4. Cd 3d XPS spectrum for the $Cu_2Cd_{0.47}Zn_{0.53}SnS_4$ alloy thin film.

C. Electrical properties of CCZTS alloy thin films

The electrical transport properties of the CCZTS alloy thin films are summarized in Table II. All samples show *p*-type conduction behaviors. The resistivity (hole carrier concentration) of the samples monotonously increases (decreases) with the higher Cd content, which can be ascribed to the compensation of acceptor defects. It has been reported that Cu substituting Zn site (Cu_{Zn}) are the main type of acceptor defects in stoichiometric CZTS and responsible for the p-type conduction of CZTS due to their low formation energies and shallow level.[9] However, in our present work, all films show the Cu-poor compositions instead of stoichiometric condition. Therefore, besides Cu_{Zn}, there is also a large amount of Cu vacancies (V_{Cu}) as acceptors in these films. As Cd alloyed into CZTS, Cd substituting Cu site (Cd_{Cu}) as donor-type doping can compensate V_{Cu} and Cu_{Zn} through forming $Cd_{Cu} + V_{Cu}$ and $Cd_{Cu} + Cu_{Zn}$ complexes.[30,36] As a result, hole concentration decreases with the Cd concentration, and the conduction concurrently becomes weaker.

D. Power conversion efficiency of CCZTS-based film solar cells

In order to comparatively study the performance of solar cells based on CCZTS without and with Cd, we prepared two prototype devices with a typical structures of ZnO:Al/ZnO/CdS/CCZTS/Mo. The Cd contents in the absorbed layers of solar cells are 0 and 0.47, respectively, denoted as devices A and B. Figure 6 shows the *I-V* curves of both devices under 100 mW/cm^2 simulated AM1.5 solar illumination. The performance parameters of both devices are also shown in Fig. 6. The device B shows a power conversion efficiency of 1.2%, higher than the device A (0.7%), which is due to the larger filled factor (*FF*) and short circuit current (I_{SC}). Furthermore, the open circuit voltage of the device B, $V_{OC} = 333.2$ mV, is lower than that of the device A ($V_{OC} = 417.1$ mV), in line with the approximately

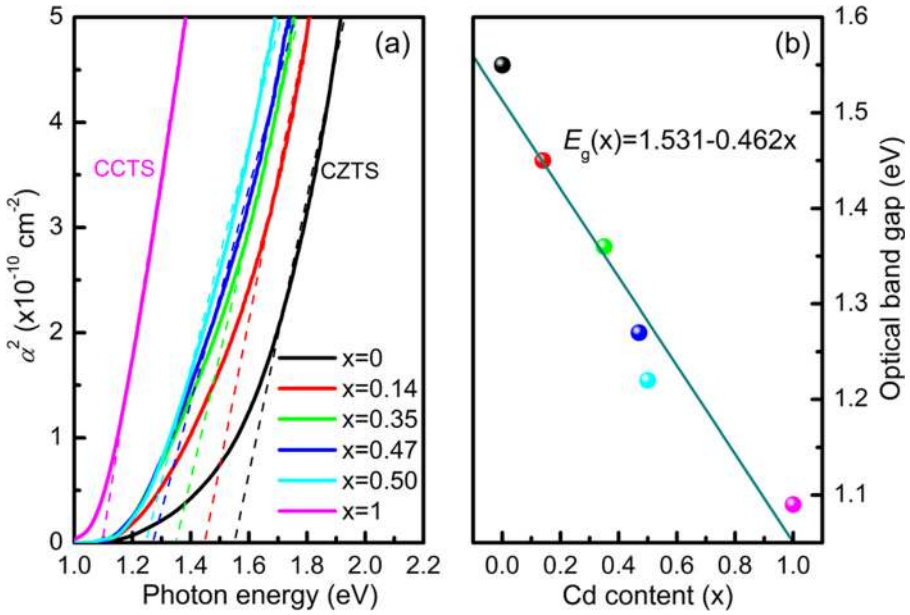

FIG. 5. (a) Room-temperature optical absorption spectra of $Cu_2Cd_xZn_{1-x}SnS_4$ alloy thin films. (b) Dependence of the optical bandgap of $Cu_2Cd_xZn_{1-x}SnS_4$ alloy films on the Cd content. The solid line is the linear fitting to the data.

TABLE II. Electrical properties of the $Cu_2Cd_xZn_{1-x}SnS_4$ alloy thin films.

Cd/(Cd + Zn) in solution	Cd/(Cd + Zn) in film	Resistivity (Ωcm)	Carrier Conc. (cm^{-3})	Mobility (cm^{2}V^{-1}s^{-1})	Carrier type
0	0	0.29	4.4×10^{20}	0.05	p
0.1	0.14	0.3	3.6×10^{20}	0.03	p
0.3	0.35	10.0	9.1×10^{19}	0.01	p
0.5	0.47	1.1×10^2	1.0×10^{17}	0.5	p
0.8	0.50	7.0×10^2	4.6×10^{16}	0.2	p

proportional relation between V_{OC} and E_g.[45,46] Although the power conversion efficiency of these devices is quite low without elaborate optimization, our preliminary results suggest that the performance of CCZTS-based solar cells is quite tunable at varied Cd content. In future studies, it is important to carefully consider the trade-off between various parameters and design tandem solar cells with the optimal performance.

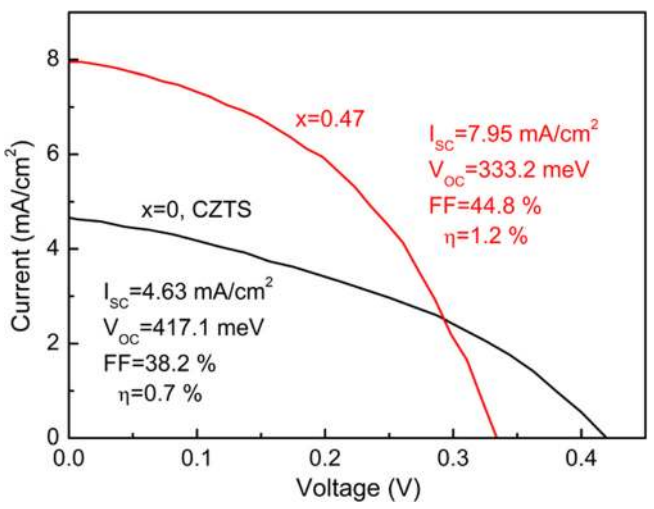

FIG. 6. *I–V* characteristics for the ZnO:Al/ZnO/CdS/CCZTS/Mo solar cell with the Cd content x = 0 and 0.47.

E. Electronic structure of CCZTS and band-alignment of CZTS/CCTS

Figures 7(a) and 7(b) show the calculated band structures of the two end compounds of CZTS and CCTS. The VBM of the CZTS is selected as the energy reference ($E_{VBM} = 0$). It is found that the bandgap of CCTS is significantly smaller than CZTS. The calculated bandgaps of CCZTS alloys as a function of Cd content are shown in Fig. 7(c). The bandgap decreases with the increase of Cd content, and the trend is well consistent with the experimentally obtained optical bandgap and supports our experimental results. It should be noted that, although the first-principles calculation systematically underestimates the magnitude of bandgap, as documented by such studies in literature,[16] it does not affect our discussions here. Furthermore, the CZTS/CCTS interface shows the type-I band alignment, as shown in Figs. 7(a) and 7(b). We found a small VBO for the CZTS/CCTS system: The VBM of CCTS is only 0.011 eV above the VBM of CZTS. For CCZTS alloy with *p*-type conduction, a small VBO at interface is clearly favorable for charge transport, benefiting the current match at the interface.

To better understand the valence-band offset (VBO) of CZTS and CCTS, we calculated their density of states (DOS) based on the hybrid functional method. Figures 8(a) and 8(b) show the total and partial VB DOS of CZTS and CCTS, respectively. To test validity of our calculation, the XPS spectral line of CZTS in the VB region is also shown in

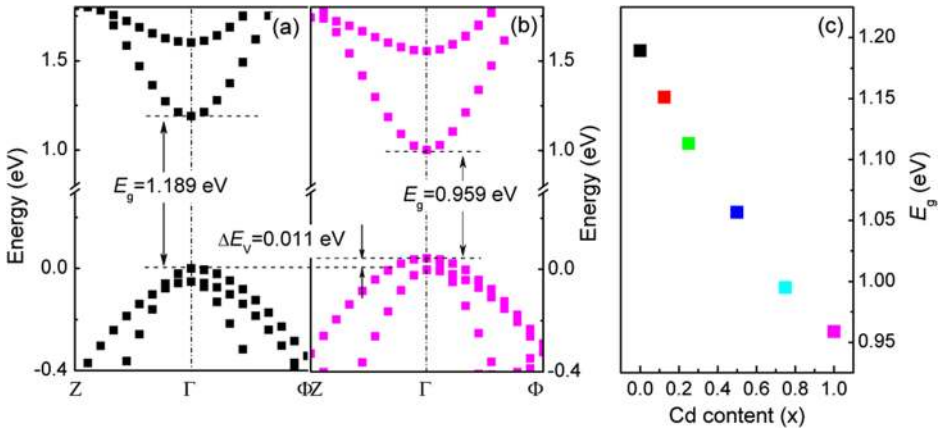

FIG. 7. Band structures of (a) Cu_2ZnSnS_4 and (b) Cu_2CdSnS_4 based on the hybrid functional first-principles calculations. (c) Calculated band gap of $Cu_2Cd_xZn_{1-x}SnS_4$ alloy as function of Cd content.

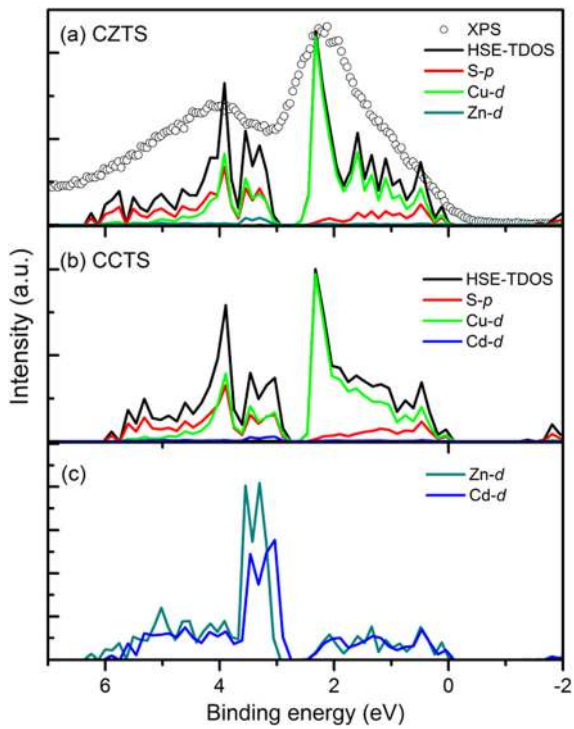

FIG. 8. Total and partial DOS in the VB regions of (a) CZTS and (b) CCTS. (c) Partial DOS of Zn-*d* and Cd-*d* for CZTS and CCTS. For comparison, the experimental XPS spectrum in the VB region of the CZTS film is also shown in (a).

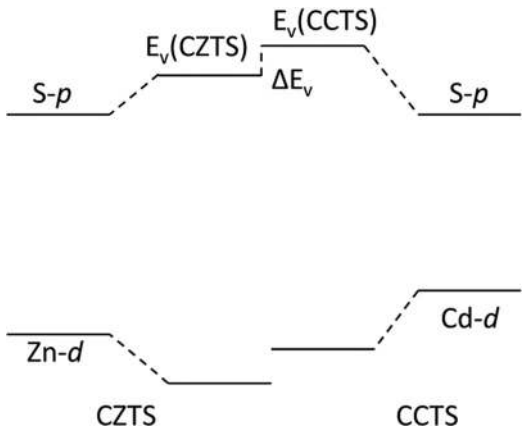

FIG. 9. Schematic diagram of the *p–d* repulsion effects on the valence band offset of CZTS/CCTS system.

Fig. 8(a). XPS spectral line in the VB region usually can provide some useful information of VB DOS. Indeed, the calculated DOS is in good agreement with the overall shape of the XPS spectrum, indicating that the results of our calculations are reliable. Based on our calculations, we found that (i) S-*p* state is one of the key components of the VBM DOS and (ii) there are shallow occupied Zn-*d* and Cd-*d* states in the VB region for CZTS and CCTS, respectively. To clearly illustrate this effect, the enlarged view of the corresponding Zn-*d* and Cd-*d* states is shown in Fig. 8(c). It is found that the Cd-*d* state is slightly shallower than Zn-*d* one.

In general, for the common-anion systems, such as CZTS and CCTS discussed here, in their VB regions, the shallower cation *d* band repels the anion *p* band upwards more than the deeper cation *d* band. Thus, the VBM of the CCTS is located at a higher energy than that of CZTS, as shown in Figs. 8(a) and 8(b). On the other hand, the longer bond length of CCTS due to the larger lattice constant leads to a weaker *p-d* repulsion and counteracts the upwards movement of VBM. Consequently, a slightly higher VBM of CCTS compared to that of CZTS is obtained. Figure 9 shows a schematic diagram of the effect of *p-d* repulsion on the band alignment. The CCZTS alloys with intermediate Cd doping levels can be considered using the same principles, and the valence band offset in tandem solar cells is expected to vary systematically.

IV. CONCLUSION

In summary, we fabricated the CCZTS alloy films with different Cd contents with single kesterite phase using the sol-gel method. The optical band gap of the kesterite CCZTS alloy can be modulated continuously from 1.55 to 1.09 eV as Cd varies from $x = 0$ to 1, suggest that the CCZTS alloy is a potentially suitable material to fabricate future high-efficiency multi-junction solar cells with different bandgap-tailored absorption layers. The power conversion efficiency of the CCZTS-based solar cell with a Cd doping concentration of 0.47 is 1.2%, higher than the one without Cd. Based on first-principles calculations, we found that CZTS/CCTS interface exhibits the type-I band alignment with a small VBO, and our results can also explain the narrowing of the bandgap of CCZTS as the Cd content increases. The upward shift of the VBM energy of CCTS with respect to that of

CZTS is attributed to the stronger *p-d* repulsion in CCTS. Overall, it is clear that Cd doping has a notable tuning effect on the band structure of the kesterite-structured CZTS alloys, and the insights provided here hopefully can lead to the construction of future tandem solar cells.

ACKNOWLEDGMENTS

This work was supported by the National Natural Science Foundation of China under Grant Nos. 10874178, 11074093, 61205038, and 11274135, Natural Science Foundation of Jilin province under Grant No. 201115013, and National Found for Fostering Talents of Basic Science under Grant No. J1103202, and Ph.D. Programs Foundation of Ministry of Education of China under Grant No. 20120061120011. This work was supported by High Performance Computing Center of Jilin University, China.

[1]Y.-H. Su, Y.-F. Ke, S.-L. Cai, and Q.-Y. Yao, Light: Sci. Appl. **1**, e14 (2012).
[2]W. J. E. Beek, M. M. Wienk, and R. A. J. Janssen, Adv. Mater. **16**, 1009 (2004).
[3]E. D. Kosten, J. H. Atwater, J. Parsons, A. Polman, and H. A. Atwater, Light: Sci. Appl. **2**, e45 (2013).
[4]K. Ramanathan, G. Teeter, J. C. Keane, and R. Noufi, Thin Solid Films **480**, 499 (2005).
[5]S. S. Schmidt, D. Abou-Ras, S. Sadewasser, W. Yin, C. Feng, and Y. Yan, Phys. Rev. Lett. **109**, 095506 (2012).
[6]C. Wadia, A. P. Alivisatos, and D. M. Kammen, Environ. Sci. Tech. **43**, 2072 (2009).
[7]B. Shin, O. Gunawan, Y. Zhu, N. A. Bojarczuk, S. J. Chey, and S. Guha, Prog. Photovoltaics **21**, 72 (2013).
[8]C. Tablero, J. Phys. Chem. C **116**, 23224 (2012).
[9]A. Walsh, S. Chen, S.-H. Wei, and X.-G. Gong, Adv. Energy Mater. **2**, 400 (2012).
[10]T. Todorov and D. B. Mitzi, Eur. J. Inorg. Chem. **2010**, 17 (2010).
[11]J.-S. Seol, S.-Y. Lee, J.-C. Lee, H.-D. Nam, and K.-H. Kim, Sol. Energy Mater. Sol. Cells **75**, 155 (2003).
[12]K. Tanaka, Y. Fukui, N. Moritake, and H. Uchiki, Sol. Energy Mater. Sol. Cells **95**, 838 (2011).
[13]L. Sun, J. He, H. Kong, F. Yue, P. Yang, and J. Chu, Sol. Energy Mater. Sol. Cells **95**, 2907 (2011).
[14]S. Schorr, Sol. Energy Mater. Sol. Cells **95**, 1482 (2011).
[15]T. Rath, W. Haas, A. Pein, R. Saf, E. Maier, B. Kunert, F. Hofer, R. Resel, and G. Trimmel, Sol. Energy Mater. Sol. Cells **101**, 87 (2012).
[16]C.-R. Li, Y.-F. Li, B. Yao, G. Yang, Z.-H. Ding, R. Deng, and L. Liu, Phys. Lett. A **377**, 2398 (2013).
[17]T. Kato, H. Hiroi, N. Sakai, S. Muraoka, and H. Sugimoto, "Characterization of front and back interfaces on Cu2ZnSnS4 thin-film solar cells," in *27th European Photovoltaic Solar Energy Conference and Exhibition* (2012), p. 2236.
[18]M. Schmid, R. Caballero, R. Klenk, J. Krč, T. Rissom, M. Topič, and M. C. Lux-Steiner, EPJ Photovolt. **1**, 10601 (2010).
[19]M. Meusel, C. Baur, G. Letay, A. W. Bett, W. Warta, and E. Fernandez, Prog. Photovoltaics **11**, 499 (2003).
[20]N. J. Ekins-Daukes, K. W. J. Barnham, J. P. Connolly, J. S. Roberts, J. C. Clark, G. Hill, and M. Mazzer, Appl. Phys. Lett. **75**, 4195 (1999).
[21]H. K. Kang, S.-H. Park, D. H. Jun, C. Z. Kim, K. M. Song, W. Park, C. G. Ko, and H. Kim, Semicond. Sci. Technol. **26**, 075009 (2011).
[22]Y. F. Li, B. Yao, Y. M. Lu, C. X. Cong, Z. Z. Zhang, Y. Q. Gai, C. J. Zheng, B. H. Li, Z. P. Wei, D. Z. Shen, X. W. Fan, L. Xiao, S. C. Xu, and Y. Liu, Appl. Phys. Lett. **91**, 021915 (2007).
[23]Y. F. Li, B. Yao, Y. M. Lu, Y. Q. Gai, C. X. Cong, Z. Z. Zhang, D. X. Zhao, J. Y. Zhang, B. H. Li, D. Z. Shen, X. W. Fan, and Z. K. Tang, J. Appl. Phys. **104**, 083516 (2008).
[24]G. Kresse and D. Joubert, Phys. Rev. B **59**, 1758 (1999).
[25]P. E. Blöchl, Phys. Rev. B **50**, 17953 (1994).
[26]J. P. Perdew, K. Burke, and M. Ernzerhof, Phys. Rev. Lett. **77**, 3865 (1996).
[27]J. Heyd, G. E. Scuseria, and M. Ernzerhof, J. Chem. Phys. **118**, 8207 (2003).
[28]G. Kresse and J. Furthmüller, Phys. Rev. B **54**, 11169 (1996).
[29]G. Kresse and J. Furthmüller, Comput. Mater. Sci. **6**, 15 (1996).
[30]T. Maeda, S. Nakamura, and T. Wada, Jpn. J. Appl. Phys., Part 1 **51**, 10NC11 (2012).
[31]R. Deng, B. Yao, Y. F. Li, Y. M. Zhao, B. H. Li, C. X. Shan, Z. Z. Zhang, D. X. Zhao, J. Y. Zhang, D. Z. Shen, and X. W. Fan, Appl. Phys. Lett. **94**, 022108 (2009).
[32]T. M. Duc, C. Hsu, and J. P. Faurie, Phys. Rev. Lett. **58**, 1127 (1987).
[33]S. P. Kowalczyk, J. T. Cheung, E. A. Kraut, and R. W. Grant, Phys. Rev. Lett. **56**, 1605 (1986).
[34]S.-H. Wei and A. Zunger, Appl. Phys. Lett. **72**, 2011 (1998).
[35]Y. F. Li, B. Yao, Y. M. Lu, B. H. Li, Y. Q. Gai, C. X. Cong, Z. Z. Zhang, D. X. Zhao, J. Y. Zhang, D. Z. Shen, and X. W. Fan, Appl. Phys. Lett. **92**, 192116 (2008).
[36]S. Chen, X. G. Gong, A. Walsh, and S.-H. Wei, Appl. Phys. Lett. **96**, 021902 (2010).
[37]J. Paier, R. Asahi, A. Nagoya, and G. Kresse, Phys. Rev. B **79**, 115126 (2009).
[38]M. Polak, J. Electron Spectrosc. Relat. Phenom. **28**, 171 (1982).
[39]W. J. Danaher, L. E. Lyons, M. Marychurch, and G. C. Morris, Appl. Surf. Sci. **27**, 338 (1986).
[40]S. C. Riha, B. A. Parkinson, and A. L. Prieto, J. Am. Chem. Soc. **131**, 12054 (2009).
[41]Y. Li, R. Deng, B. Yao, G. Xing, D. Wang, and T. Wu, Appl. Phys. Lett. **97**, 102506 (2010).
[42]Y. F. Li, B. Yao, Y. M. Lu, Z. P. Wei, Y. Q. Gai, C. J. Zheng, Z. Z. Zhang, B. H. Li, D. Z. Shen, X. W. Fan, and Z. K. Tang, Appl. Phys. Lett. **91**, 232115 (2007).
[43]K. Ito and T. Nakazawa, Jpn. J. Appl. Phys., Part 1 **27**, 2094 (1988).
[44]H. Katagiri, K. Saitoh, T. Washio, H. Shinohara, T. Kurumadani, and S. Miyajima, Sol. Energy Mater. Sol. Cells **65**, 141 (2001).
[45]V. Nadenau, U. Rau, A. Jasenek, and H. W. Schock, J. Appl. Phys. **87**, 584 (2000).
[46]T. K. Todorov, J. Tang, S. Bag, O. Gunawan, T. Gokmen, Y. Zhu, and D. B. Mitzi, Adv. Energy Mater. **3**, 34 (2013).